AMERICAN SOCIETY FOR MICROBIOLOGY | Journal of Virology®

VIRUS-CELL INTERACTIONS

Ebola Virus Delta Peptide Is a Viroporin

Jing He,[a] Lilia I. Melnik,[b] Alexander Komin,[c,d] Gregory Wiedman,[c,d] Taylor Fuselier,[a] Cameron F. Morris,[a] Charles G. Starr,[a] Peter C. Searson,[c,d] William R. Gallaher,[e,f] Kalina Hristova,[c,d] Robert F. Garry,[b,g,h] William C. Wimley[a]

Department of Biochemistry and Molecular Biology, Tulane University School of Medicine, New Orleans, Louisiana, USA[a]; Department of Microbiology and Immunology, Tulane University School of Medicine, New Orleans, Louisiana, USA[b]; Department of Materials Science and Engineering, Johns Hopkins University, Baltimore, Maryland, USA[c]; Institute for NanoBioTechnology, Johns Hopkins University, Baltimore, Maryland, USA[d]; Department of Microbiology, Immunology and Parasitology, LSU Health Sciences Center, New Orleans, Louisiana, USA[e]; Mockingbird Nature Research Group, Pearl River, Louisiana, USA[f]; Zalgen Labs, LLC, Germantown, Maryland, USA[g]; Tulane Center of Excellence, Global Viral Network, New Orleans, Louisiana, USA[h]

ABSTRACT The Ebola virus (EBOV) genome encodes a partly conserved 40-residue nonstructural polypeptide, called the delta peptide, that is produced in abundance during Ebola virus disease (EVD). The function of the delta peptide is unknown, but sequence analysis has suggested that delta peptide could be a viroporin, belonging to a diverse family of membrane-permeabilizing small polypeptides involved in replication and pathogenesis of numerous viruses. Full-length and conserved C-terminal delta peptide fragments permeabilize the plasma membranes of nucleated cells of rodent, dog, monkey, and human origin; increase ion permeability across confluent cell monolayers; and permeabilize synthetic lipid bilayers. Permeabilization activity is completely dependent on the disulfide bond between the two conserved cysteines. The conserved C-terminal portion of the peptide is biochemically stable in human serum, and most serum-stable fragments have full activity. Taken together, the evidence strongly suggests that Ebola virus delta peptide is a viroporin and that it may be a novel, targetable aspect of Ebola virus disease pathology.

IMPORTANCE During the unparalleled West African outbreak of Ebola virus disease (EVD) that began in late 2013, the lack of effective countermeasures resulted in chains of serial infection and a high mortality rate among infected patients. A better understanding of disease pathology is desperately needed to develop better countermeasures. We show here that the Ebola virus delta peptide, a conserved nonstructural protein produced in large quantities by infected cells, has the characteristics of a viroporin. This information suggests a critical role for the delta peptide in Ebola virus disease pathology and as a possible target for novel countermeasures.

KEYWORDS delta peptide, Ebola virus, enterotoxins, permeabilization, viroporin

Received 20 March 2017 **Accepted** 18 May 2017

Accepted manuscript posted online 24 May 2017

Citation He J, Melnik LI, Komin A, Wiedman G, Fuselier T, Morris CF, Starr CG, Searson PC, Gallaher WR, Hristova K, Garry RF, Wimley WC. 2017. Ebola virus delta peptide is a viroporin. J Virol 91:e00438-17. https://doi.org/10.1128/JVI.00438-17.

Editor Adolfo García-Sastre, Icahn School of Medicine at Mount Sinai

Address correspondence to Robert F. Garry, rfgarry@tulane.edu, or William C. Wimley, wwimley@tulane.edu.

An unprecedented global health emergency began in December 2013 when an 18-month-old child became infected with Ebola virus (EBOV) Makona variant in the West African country of Guinea. The origin of Ebola virus in West Africa in not known, but there has been speculation that the outbreak was initiated by an epizoonotic transmission by a bat from a colony occupying a hollow tree near the child's village of Meliandou (1). The child died of Ebola virus disease (EVD), as did several members of his family and other village residents. From Meliandou, EBOV ultimately spread by human-to-human contact throughout much of Guinea, Liberia, and Sierra Leone and made incursions into other West African nations, Europe, and the United States. During the outbreak, which peaked in late 2014, more than 28,000 cases and 11,000 deaths were reported (2). Long-term persistence of EBOV in immunologically privileged compartments, such as the testes (3), eye (4), mammary glands (5), and cerebrospinal fluid (6), has been documented. A few new Ebola cases continued into 2016, including sexually

transmitted cases (7). While it is unknown whether EBOV is present in reservoir animal species throughout the forested area of West Africa, it is likely that the subregion, or other regions, will experience future reemergences of EBOV.

EVD in West Africa is characterized by fever, weakness, and severe gastrointestinal illness that causes severe fluid loss, electrolyte imbalance, and multiorgan failure (8, 9). The 2013-2016 West African outbreak of the Ebola virus variant Makona, like the small, sporadic outbreaks of other Ebola virus variants that had occurred in middle Africa over the last 40 years, had a high mortality rate because there is no effective, widely available treatment. Most EVD patients in West Africa received only limited supportive care. Progress is being made toward vaccines (10), an approach that may serve health care workers and known contacts of EVD cases. However, only modest progress was made toward direct therapeutic countermeasure development during the recent outbreak. Development of effective therapies will depend on a better understanding of EBOV pathogenesis. Toward this goal, we are characterizing the delta peptide of EBOV, a conserved segment of the Ebola virus nonstructural proteome to which no function has yet been definitively assigned.

The delta peptide is the product of variant envelope glycoprotein (GP) production, which occurs via differential mRNA editing (11, 12). As shown in Fig. 1A, editing at a genomic 7U site can add one or more untemplated adenines to the GP mRNA sequence, shifting the downstream translational reading frame. Virion-associated GP, which is encoded by an mRNA containing one additional nontemplated adenosine, traffics through the endoplasmic reticulum (ER), becomes glycosylated, and is delivered to the plasma membrane, where it is anchored by the carboxyl-terminal helical transmembrane (TM) domain. The major form of GP is the soluble secreted form (sGP), which is the product of unedited GP mRNA. This form of GP is produced in large excess over virion-associated GP (12, 13) and is likely an immune system decoy (14). It lacks much of the C-terminal portion of GP, including the membrane anchor, but contains additional carboxyl-terminal amino acids not present in full-length GP (12, 15). Intracellular processing of sGP, which includes cleavage at a furin-like protease-sensitive site that is not present in viral GP, releases mature dimeric sGP for secretion, along with the carboxyl-terminal 40-amino-acid sequence that is called the delta peptide.

Recently (16), we noted that delta peptides from various related filoviruses have a high abundance of cationic and aromatic residues and are potentially amphipathic, properties that are found in many membrane-permeabilizing peptides (17). We hypothesized that the Ebola virus delta peptide might be a viroporin, a virus-encoded small protein that can permeabilize one or more internal cell membranes, the plasma membrane of animal cells, or the viral envelope. Here, we test synthetic Ebola virus delta peptide for cell-permeabilizing and cytotoxic activities and show that it is a potent viroporin.

RESULTS AND DISCUSSION

Delta peptide of Ebola virus. Delta peptides of Ebola virus representative species are 40 to 49 residues long and are comprised of a variable N-terminal segment of 17 to 18 residues followed by a better-conserved C-terminal segment of 23 to 31 residues (Fig. 1B). Conserved residues in the C terminus include two cysteines, as well as aromatic and basic residues. There are two ways in which the Ebola virus delta peptide could form an amphipathic, membrane-active molecule. First, it has potential amphipathic character in α-helical form (16), a structural motif that drives the membrane activity of many pore-forming peptides, including some viroporins (18, 19). Second, the conserved pair of cysteine residues suggests that delta peptides could form a disulfide cross-linked hairpin structure that could also be amphipathic. Such a structure would be similar to many membrane-permeabilizing antimicrobial peptides (20). To determine whether the Ebola virus delta peptide has membrane-permeabilizing, viroporin-like activity in either of these two structural states, we made a set of EBOV delta peptide variants using the Makona variant sequence from West Africa (21). We made oxidized (disulfide cross-linked) and reduced full-length Ebola delta peptide ($E40_{ox}$ and $E40_{red}$,

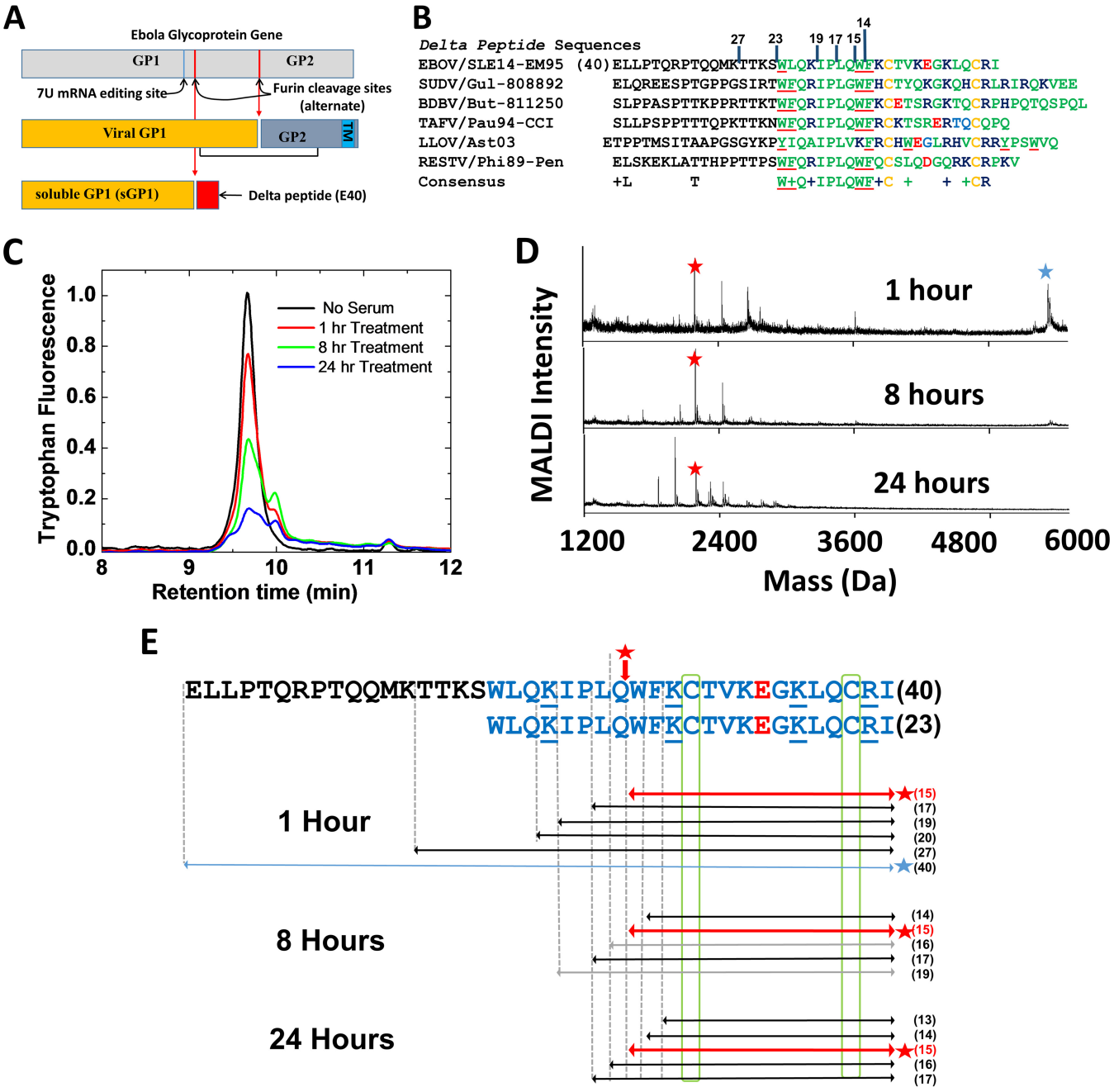

FIG 1 Ebola virus delta peptide. (A) EBOV glycoprotein editing. The GP gene can produce multiple versions of the protein due to differential RNA editing at a conserved site containing seven uridine residues. All versions share the first 295 amino acid residues. Full-length GP, which is 676 amino acids, is produced from mRNAs containing an additional nontemplated adenosine. Full-length GP is converted to GP1 and GP2 by cleavage at a furin-like protease-sensitive site and is membrane anchored by a C-terminal membrane-spanning helix domain. sGP, which is produced from the unedited RNA transcript, contains only the first 364 to 372 amino acids of the GP1 domain. The delta peptide, which is the frame-shifted C terminus of sGP, is cleaved from sGP in cells at an alternate furin-like protease site created by the RNA editing. (B) Delta peptide sequences from Ebola virus and related filoviruses. The conserved C terminus is green, except basic residues are blue, acidic residues are red, and cysteine is yellow. Aromatic residues are underlined. In the consensus sequence, a residue letter indicates that at least 6 of the 7 sequences have the same residue, while a plus sign indicates a conserved physical chemistry. (C) HPLC chromatograms of tryptophan fluorescence of Ebola virus delta peptide incubated in human serum for 1 to 24 h at 37°C. At each time point, C-terminal biotinylated delta peptide was extracted from serum using bead-immobilized streptavidin and released with 1 mM free biotin after extensive washing. The released peptide was eluted from a reverse-phase C_{18} column developed in water/acetonitrile. The data are not corrected for the number of tryptophans; therefore, the 8- and 24-h intensities per molecule are halved by the loss of tryptophan 18 by proteolysis. (D) Serum stability of $E40_{ox}$ after incubation with 10% human serum at 37°C for the indicated times. The bead wash solution was subjected to HPLC and MALDI-time of flight (TOF) mass spectrometry, where only fragments of E40 containing the C terminus were observed. The blue star marks the full-length peptide, and the red stars mark the 15-residue fragment that persists for at least 24 h. (E) Delta peptide fragments observed after incubation with 10% human serum for 1, 8, and 24 h. The blue star indicates full-length $E40_{ox}$, and the red stars and arrows indicate the stable 15-residue C-terminal fragment. The black arrows represent the most prevalent fragments, and the gray arrows represent less abundant fragments that were detected by mass spectroscopy.

respectively) (Fig. 1B), as well as oxidized and reduced forms of the conserved 23-residue C-terminal portion ($E23_{ox}$ and $E23_{red}$). For comparison, we made the equivalent full-length and C-terminal peptides from Reston virus (RESTV), a related filovirus that causes high mortality in some nonhuman primates but apparently does not cause disease in humans (22). Based on serum stability experiments, described below, we also synthesized oxidized and reduced versions of the stable 17-, 15-, and 14-residue C-terminal fragments of the Ebola virus delta peptide. For a positive control for membrane lysis, we used MelP5, a synthetically evolved gain-of-function variant of the cytolytic bee venom peptide melittin (23).

To determine if the delta peptide is biochemically stable in serum, we assessed the resistance of oxidized delta peptide to proteolytic degradation in human serum. While the N-terminal portion of $E40_{ox}$ is rapidly degraded in serum, disulfide cross-linked C-terminal fragments between 27 and 14 residues long are resistant to serum proteolysis, as shown in Fig. 1C to E. Even after 24 h in serum, C-terminal fragments containing 13 to 17 residues remained intact. It is thus reasonable to postulate that delta peptides could have a role in human pathology of EVD and that this role could be intracellular, extracellular, or both. Peptide sequences are shown schematically in Fig. 2.

Permeabilization of cellular membranes. To assess permeabilization of mammalian cells in culture, we measured the entry of Sytox green, a small, cationic, membrane-impermeant DNA-binding dye that becomes fluorescent only if it is allowed to cross the plasma membrane. In a few experiments, we also examined the efflux of calcein AM ester red orange (CAMRO), a small anionic dye that is membrane impermeant once activated by cytosolic esterases. In control samples, most cells exclude Sytox green and retain CAMRO for hours. When cells are permeabilized, Sytox green enters and CAMRO exits the cytosol (Fig. 3A).

Given the lack of long-term selective pressure in the rare human host prior to an EVD outbreak, we hypothesized that if delta peptides contribute to disease pathology in humans, they do so without highly sequence-specific interactions with human proteins. To test this hypothesis, we measured membrane-permeabilizing activity in four nucleated mammalian cell types; rodent (CHO), canine (MDCK), human (HeLa), and nonhuman primate (Vero) cells. Ebola virus is able to infect and propagate in the last two cell types in the laboratory (24). When added to mammalian cells in culture, $E40_{ox}$ permeabilizes plasma membranes to Sytox green with a half-life ($t_{1/2}$) of about 10 min (Fig. 3B) and with a 50% effective concentration (EC_{50}) of 5 to 25 μM (Fig. 3C to F and Table 1). Cells from rodents, dogs, monkeys, and humans are all susceptible to delta peptide permeabilization (Table 1). MDCK cells were the most susceptible, while Vero cells were the least, but the total variation was small. For comparison, the highly potent cytolytic peptide MelP5 permeabilized the same cells with a $t_{1/2}$ of 10 min and an EC_{50} of 1 to 3 μM. Oxidized, truncated C-terminal delta peptides of 23, 17, and 15 residues were similarly active (Fig. 3 and Table 1).

As shown in Table 1 and Fig. 3, the oxidized 14-residue C-terminal variant, $E14_{ox}$, is inactive in all cell types. Because it shares many residues with and is treated identically to the active variants, it serves as a negative control. Similarly, all the reduced delta peptides studied (E40, E23, E17, E15, and E14) were essentially inactive in all cell types (Table 1 and Fig. 3), providing additional negative controls. We conclude that the cell-permeabilizing activity of the Ebola virus delta peptides (i) resides in the more conserved C terminus of the sequence, (ii) is completely dependent on the disulfide cross-linked C-terminal hairpin structure (Fig. 2), and (iii) is completely dependent on the presence of the tryptophan that is 15 residues from the C terminus.

Oxidized Reston virus delta peptides, full-length $R42_{ox}$ and C-terminally truncated $R25_{ox}$, were less potent than $E40_{ox}$ and $E23_{ox}$ in these experiments (Table 1). $E42_{ox}$ had little measurable activity, while $R25_{ox}$ had EC_{50} values, where tested, of 50 to 70 μM compared to 10 to 20 μM for $E23_{ox}$. The observations that the C-terminal fragment, R25, contains the cell-permeabilizing activity and that its activity is lost upon reduction

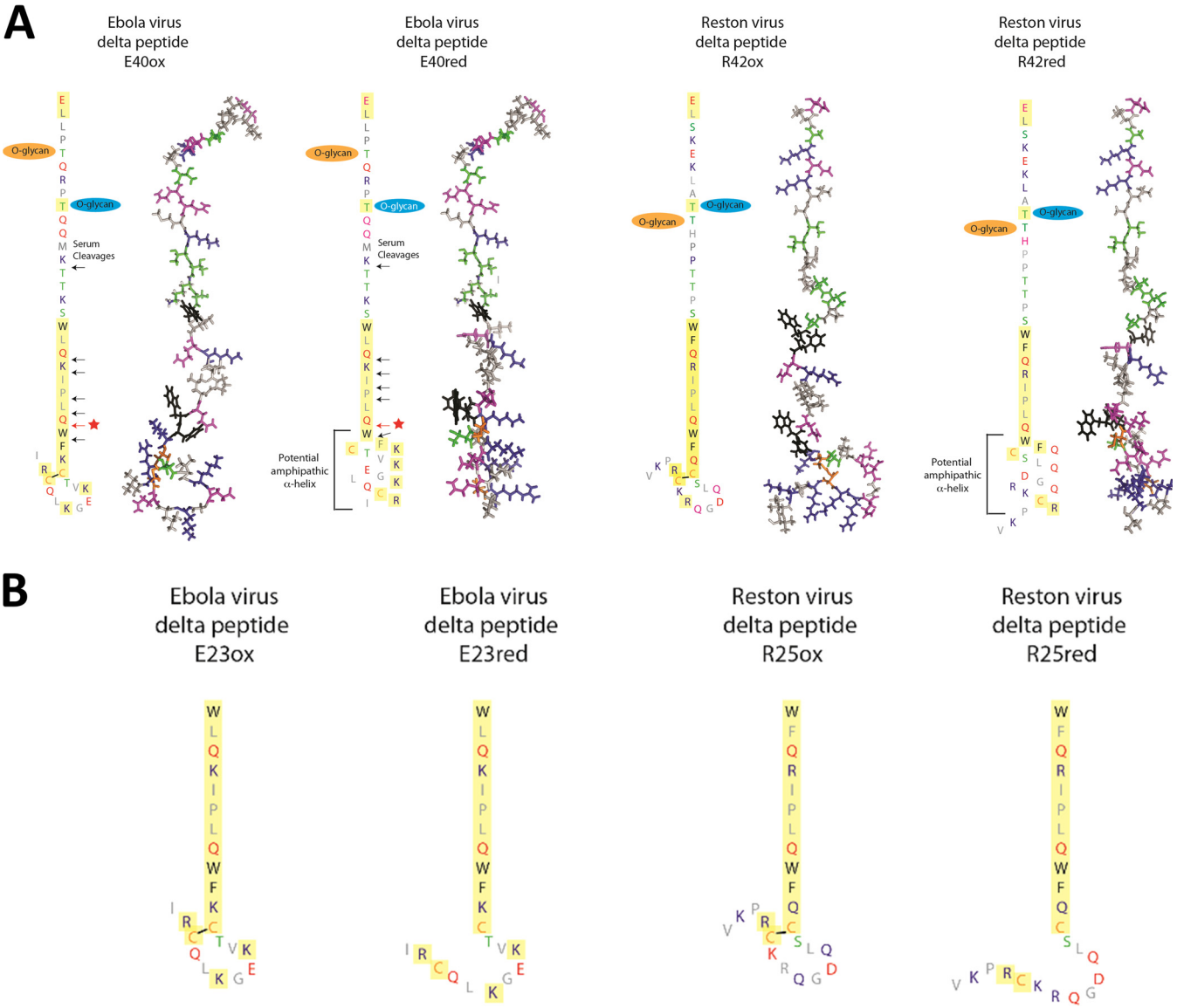

FIG 2 Schematic representations of filovirus delta peptides. (A) Full-length Ebola virus delta peptide (left two structures) is a 40-residue peptide that is cleaved from the soluble glycoprotein during processing. The delta peptide is glycosylated near the N terminus. The C-terminal 23 residues (yellow) are well conserved among related viruses. This C-terminal domain could form amphipathic structures as a disulfide cross-linked hairpin (left structure of each pair) or as an amphipathic helix (right). The Reston virus delta peptide, (right two structures), which is 42 residues long, has similar properties. Observed sites of cleavage by serum proteases are indicated by arrows, with the starred red arrow designating the 15-residue C-terminal fragment that remains intact even after 24 h at 37°C in serum. (B) The 23-residue Ebola virus peptide and 25-residue Reston peptide fragments that represent the more conserved C-terminal half of the peptide. These peptides retain the activity of the full-length peptide when oxidized.

suggests that the RESTV delta peptide has a biological activity that is related to that of the Ebola virus delta peptide. Similarly, the fact that 12 of 23 C-terminal residues (52%) are identical between the two sequences and 18 of 23 residues (78%) are either identical or very similar also suggests similar biological activity. The sequence differences do not suggest an obvious hypothesis as to why RESTV delta peptides were less active than EBOV delta peptides in these experiments. However, we note that Sytox green is a surrogate measurement for membrane permeabilization that may not precisely mimic the biological activity.

We verified the cell permeabilization by EBOV delta peptides by measuring the effects of E40 and E23 on transendothelial electrical resistance (TEER) across a confluent monolayer of MDCK cells. We observed that $E40_{ox}$ and $E23_{ox}$, along with the MelP5 positive control, readily permeabilized cell monolayers, while $E40_{red}$ and $E23_{red}$ did not

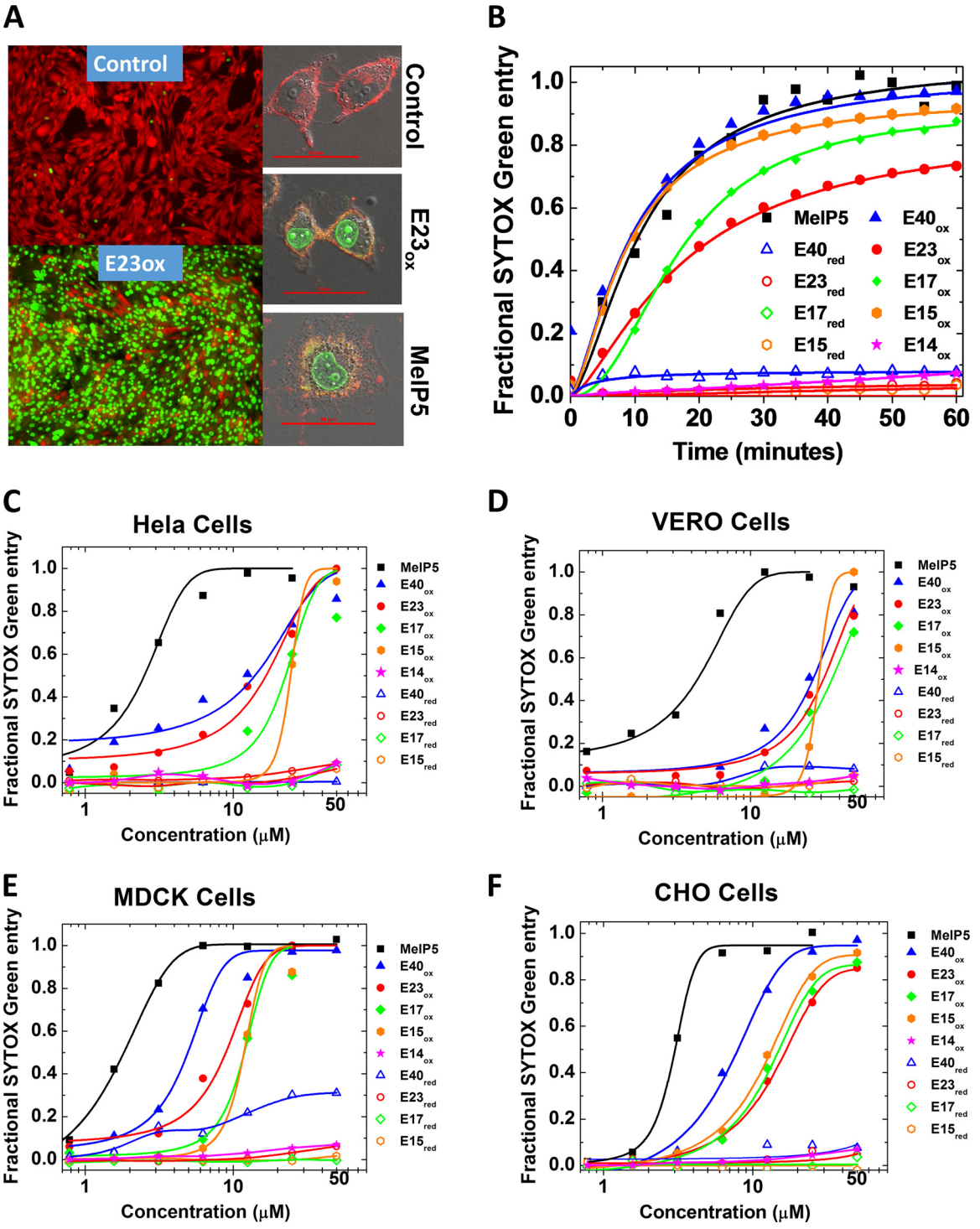

FIG 3 Permeabilization of cell membranes by delta peptides. (A) (Left) Example epifluorescence images of cells incubated with CAMRO and Sytox green. CAMRO enters the cytosol, where it is converted to the fluorescent and membrane-impermeant dye (red). Sytox green is a membrane-impermeant DNA-binding dye that becomes fluorescent only if it can access the nucleus due to plasma membrane disruption. Intact cells are red, and cells permeable to both dyes are green. The lower image shows cells treated with 50 μM $E23_{ox}$ for 1 h. (Right) Example confocal microscopy images of cells labeled with rhodamine-18, which labels membranes, and Sytox green, which fluoresces in the nucleus if cells are permeabilized. The cells were treated with buffer only, 40 μM $E23_{ox}$, or 5 μM MelP5. Scale bars, 50 μm. (B) Time dependence of peptide-induced plasma membrane permeabilization of CHO cells as measured by Sytox green fluorescence. Delta peptides are all present at 25 μM and MelP5 is present at 5 μM. (C to F) Sytox green experiments for all cell types studied. Cells were seeded into 96-well tissue culture plates and grown to 80 to 90% confluence for 24 to 48 h in full medium. Five minutes before the addition of peptide, 100 nM Sytox green was added. The peptides were first serially diluted and then added to the cells. Sytox green fluorescence at 60 min was used to calculate fractional permeabilization of the plasma membrane. The curves are fitted with a sigmoidal function to determine the EC_{50} from the curve midpoint.

TABLE 1 Cell permeabilization

Cell type	EC_{50}[a] (μM)											
	EBOV peptides							RESTV peptides				
	$E40_{ox}$	$E40_{red}$	$E23_{ox}$	$E23_{red}$	$E17_{ox}$	$E15_{ox}$	$E14_{ox}$	$R42_{ox}$	$R42_{red}$	$R25_{ox}$	$R25_{red}$	MelP5[b]
MDCK	5.5	I	11	I	14	16	I	ND	ND	ND	ND	2.8
MDCK[c]	25	I	72	I	ND	ND	ND	ND	ND	ND	ND	9.0
HeLa	19	I	16	I	15	21	I	ND	ND	ND	ND	3.1
Vero	20	I	22	I	52	37	I	I	I	56	I	3.6
Vero[d]	18	ND	11	ND	ND	ND	ND	100	ND	49	ND	1.0
CHO	5.4	I	17	I	15	21	I	I	I	68	I	1.6
RBC[e]	>200	ND	>200	ND	>200	>200	I	I	ND	>200	ND	3.6

[a]EC_{50}, concentration required for 50% lytic or toxic effect. Oxidized EBOV or RESTV peptides (ox) have a disulfide cross-link between the conserved cysteines, while reduced peptides (red) do not. Except where noted, all measurements are based on Sytox green entry into cells after 1 h of incubation of serially diluted peptide with a cell monolayer in the presence of 100 nM Sytox green. Sytox green entry, which does not occur in unperturbed cells, is measured by the dramatically increased fluorescence of the probe when it binds to nuclear DNA (Fig. 3). I, less than 5% permeabilization was observed at the highest concentration studied, 200 μM for hemolysis and 50 or 100 μM for Sytox green entry; >200, more than 5% hemolysis was observed at the highest concentration, but the EC_{50} is greater than 200 μM peptide; ND, the experiment was not done. All values are the means of the results of ≥3 experiments. The standard deviations had an average value of 30% of the EC_{50}s listed.

[b]MelP5 is a lytic control peptide derived from the bee venom toxin, melittin (23).

[c]Loss of transepithelial electrical resistance in a confluent monolayer of MDCK cells.

[d]Cytotoxicity of peptides after 24 h of incubation with VERO cells, measured using alamarBlue fluorescence.

[e]Hemolysis of human erythrocytes, measured by assessing the peptide-induced release of hemoglobin.

(Fig. 4A and Table 1). These results are consistent with permeabilization of cultured cells to Sytox green.

We also measured the effects of delta peptides on longer timescales by measuring cytotoxicity in Vero cells incubated with delta peptides for 24 h. The EC_{50}s for cytotoxicity shown in Table 1 are similar to the values for acute permeabilization. This result shows that delta peptide permeabilization exerts a significant long-term physiological effect on cells, even at low concentrations. Permeabilization, as assayed by Sytox green entry, is not a transient effect.

Pore size in membranes. When cultured mammalian cells are treated with the lytic toxin MelP5, they swell rapidly, become spherical, and detach from cell culture surfaces, consistent with an osmotic lysis mechanism driven by the formation of large, unrestricted membrane pores (25). In contrast, cells treated with oxidized delta peptides do not swell dramatically and do not rapidly lose their shape or surface adherence (Fig. 3A and 4C), suggesting that delta peptides form smaller and more selective pores. We tested this hypothesis further by comparing Sytox green permeabilization of nucleated cells to the release of hemoglobin from human erythrocytes (hemolysis). The latter permeabilization process requires a substantial membrane pore that enables water influx and osmotic lysis (26). The control peptide MelP5, which forms large pores (25), permeabilizes nucleated cells and lyses erythrocytes with very similar, low-micromolar EC_{50}s of less than 4 μM. On the other hand, Ebola virus delta peptides, which permeabilize nucleated cells to Sytox green at 5 to 25 μM, are essentially inactive against red blood cells (RBC) in hemolysis assays up to 200 μM (Table 1 and Fig. 4B), indicating that they form small pores that do not allow uncontrolled water influx. To further test the hypothesis, we used confocal microscopy to study the peptide-induced entry of macromolecules of 3, 10, and 38 kDa molecular mass into nucleated cells. MelP5 and $E23_{ox}$ were tested in CHO cells at 2 times the EC_{50}, or 6 and 30 μM, respectively, and >95% of the cells were Sytox green positive in both cases (Table 1). At this concentration, MelP5 readily enabled equilibration of all three macromolecules across the plasma membranes of most cells (Fig. 4C and D). On the other hand, $E23_{ox}$, at a peptide concentration at which Sytox green and CAMRO readily permeate membranes, did not allow entry of macromolecules into any cells, except for a small amount of entry of a dextran that was only 3 kDa.

Permeabilization of synthetic bilayers. By measuring Sytox green entry into cells from multiple animal species, we effectively tested the hypothesis that the biological activity of the delta peptides is due to the peptide physical chemistry and is not

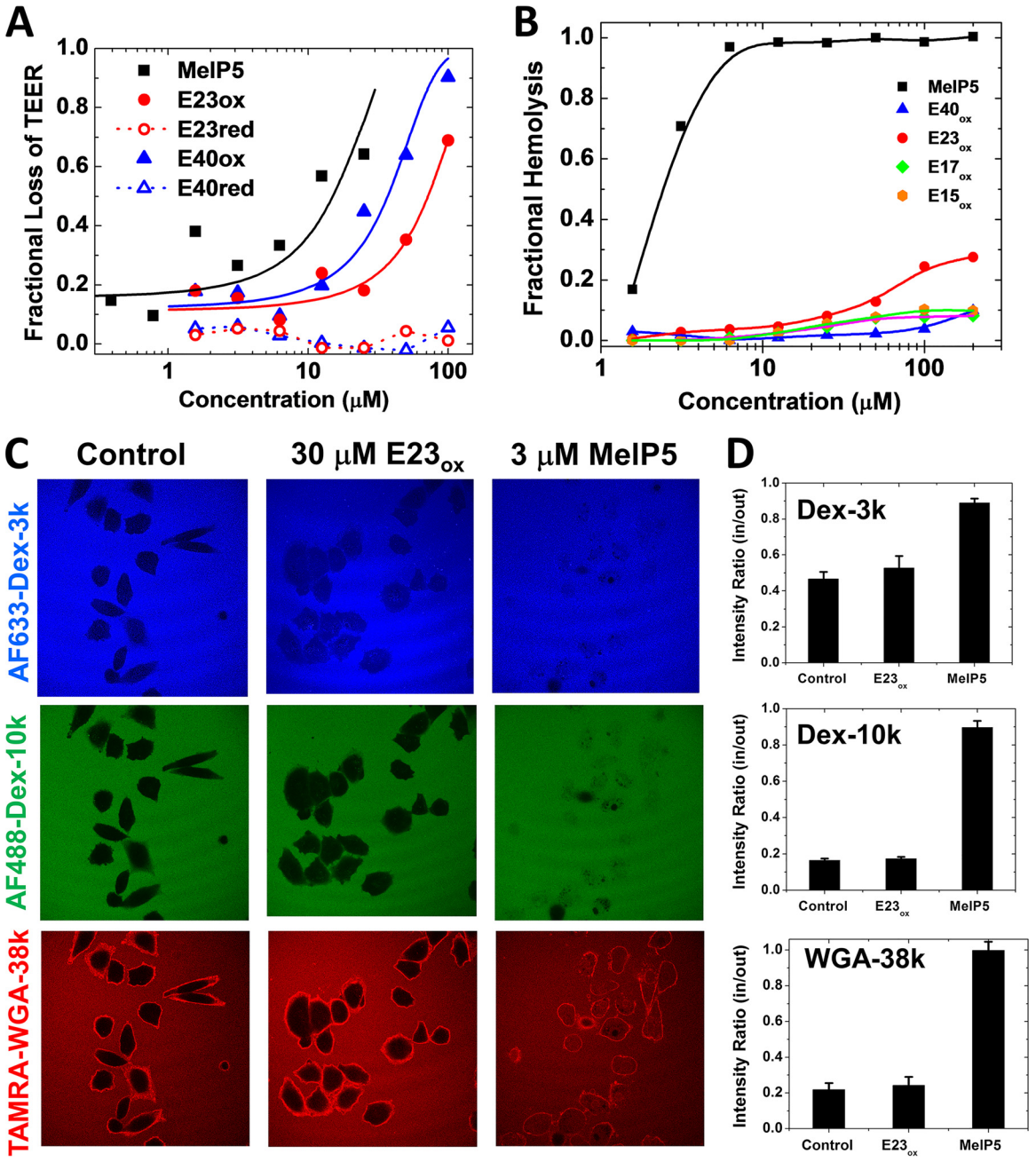

FIG 4 Mechanism of cell permeabilization. (A) Peptide-induced loss of transepithelial electrical resistance in a high-resistance, confluent monolayer of MDCK cells. The cells were treated with peptides, and TEER was measured for 1 h. Resistance at 60 min minus background resistance without cells is plotted as a fraction of the initial resistance minus background. In all experiments, the control for 100% cell permeabilization was MelP5. (B) Lysis of human erythrocytes. Fresh human red blood cells at 2×10^8 RBC/ml were incubated with serially diluted peptides. After incubation for 1 h at 37°C, the cells were centrifuged and the released hemoglobin in the supernatant was measured by optical absorbance of the heme group (410 nm). The negative control was buffer only (0% lysis), and the positive control was distilled water (100% lysis). While MelP5 is lytic at 1 to 3 μM, even 200 μM delta peptides cause only slight hemolysis. (C) Peptide-induced entry of macromolecules. CHO cells were simultaneously incubated with Alexa Fluor 633-dextran-3k (blue), Alexa Fluor 488-dextran-10k (green), and 6-carboxytetramethylrhodamine (TAMRA)-wheat germ agglutinin (WGA) (39 kDa; red). Buffer or peptides at 2 times the EC_{50} were added, and the cells were incubated for 1 h, followed by imaging by fluorescence scanning confocal microscopy. (D) Intensities inside and outside cells were measured with ImageJ for 20 to 25 cells in at least two independent fields. The error bars indicate standard deviations (SD).

dependent on sequence-specific interactions with channels, receptors, or other cell surface proteins. To test this idea further, we studied the permeabilization of synthetic lipid bilayers. First, we used electrochemical impedance spectroscopy on polymer-cushioned supported bilayers (27) to probe the effects of peptides on membrane

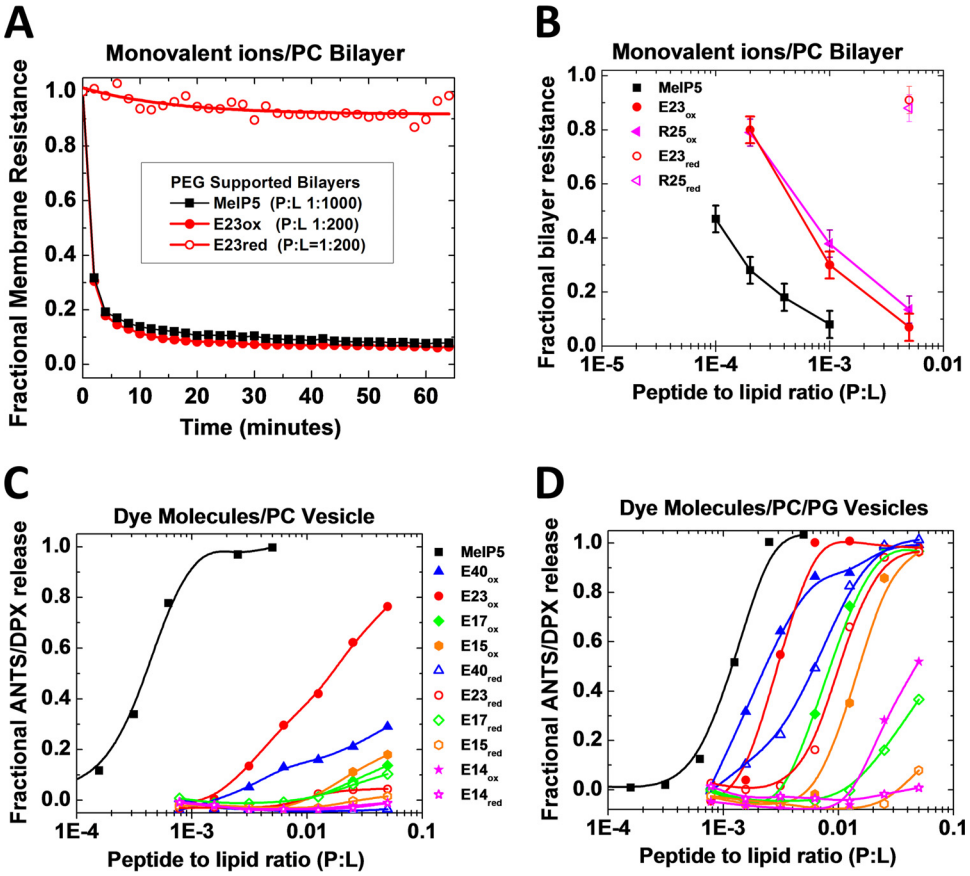

FIG 5 Permeabilization of synthetic bilayers. (A) Electrochemical impedance spectroscopy using polymer-cushioned, surface-supported PC bilayers made by Langmuir-Blodgett deposition on single-crystal silicon. Bilayer resistance is determined by fitting an equivalent circuit to spectra collected at 1-min intervals after addition of peptide at time zero. Peptide-to-lipid ratios are for the whole system, including vesicles in solution that are in equilibrium with the surface-supported bilayer. Resistance, in this experiment, is based on the movement of monovalent ions, such as Na^+, Cl^-, H^+, and OH^-, or Ca^{2+} and Mg^{2+}, across the bilayer. (B) Fractional loss of supported bilayer resistance versus peptide concentration. The values are for measurements made 60 min after addition of peptide. (C and D) Lipid vesicle permeabilization. Large unilamellar vesicles were made by extrusion from POPC (C) and POPC plus 50% POPG (D). Vesicles contained the dye ANTS (6 mM) and its quencher, DPX (12 mM). Peptide serial dilutions were added to 0.5 mM lipid vesicles in the wells of a 96-well plate. After 1 h, ANTS fluorescence was measured, and fractional leakage was calculated relative to buffer only (0% leakage) and Triton X-100 or MelP5 at a P/L ratio of 1:50 (100% leakage). The curves are fitted with a sigmoidal function to determine EC_{50} from the curve midpoint.

resistance, determined in this technique by the movement of monovalent ions across the bilayer. Second, we measured leakage of the dye-quencher pair ANTS and DPX from lipid vesicles, a phenomenon that requires membrane disturbances large enough to release molecules with molecular masses of ~350 Da. In impedance spectroscopy, MelP5 is very potent (Fig. 5A and B), rapidly decreasing the resistance of planar lipid bilayers to ions by more than 90% at a peptide-to-lipid (P/L) ratio of ≤1:1,000. $E23_{ox}$ is also potent, with a similar 90% effect at a P/L ratio of ≤1:200. The P/L ratios that cause 50% leakage (LIC_{50} values) for MelP5 and $E23_{ox}$ are ~1:10,000 and ~1:2,000, respectively (Fig. 5B and Table 2). Reduction of the delta peptide disulfide bond eliminated the membrane-permeabilizing activity of the delta peptide, again supporting the conclusion that disulfide cross-linked secondary structure is essential for activity. In vesicle leakage experiments (Fig. 5C and D) we observed a revealing difference in behavior compared to impedance spectroscopy. For dye release from zwitterionic PC vesicles, the pore former MelP5 remains highly active, with LIC_{50} values of ~1:3,000 (Fig. 5C,and Table 2). On the other hand, the delta peptides are substantially less active compared to their potent effect on ionic resistance in supported bilayers. $E23_{ox}$ is the

TABLE 2 Permeabilization of synthetic bilayers by variants of the EBOV and RESTV delta peptides

	LIC_{50}[b]											
	EBOV peptides							RESTV peptides				
Bilayer[a]	$E40_{ox}$	$E40_{red}$	$E23_{ox}$	$E23_{red}$	$E17_{ox}$	$E15_{ox}$	$E14_{ox}$	$R42_{ox}$	$R42_{red}$	$R25_{ox}$	$R25_{red}$	MelP5[c]
PC vesicles	>50	>50	16	>50	>50	>50	>50	I	I	>50	I	0.3
PC bilayer[d]	ND	ND	0.5	I	ND	ND	ND	ND	ND	0.6	I	0.1
30% PG vesicles	6	18	3	8	ND	ND	ND	22	>50	>50	>50	1.6
50% PG vesicles	2.3	6.1	2.9	10	8.6	15	48	ND	ND	ND	ND	1.2

[a]PC vesicles and bilayers are made from 1-palmitoyl-2-oleoyl-phosphatidylcholine (POPC). PC/PG bilayers also contain 30% or 50% 1-palmitoyl-2-oleoyl-phosphatidylglycerol (POPG).

[b]LIC_{50} is the P/L ratio required to induce 50% leakage of the dyes ANTS and DPX from lipid vesicles or 50% loss of bilayer resistance in a polymer-cushioned supported lipid bilayer. The LIC_{50} values in the table are multiplied by 1,000, i.e., 1 is equivalent to an LIC_{50} (P/L ratio) of 1:1,000. >50, more than 5% leakage was observed at the highest concentration but the LIC_{50} is greater than 0.05; I (inactive), less than 5% permeabilization was observed at the highest concentration (Fig. 5). Oxidized peptides (ox) have a disulfide cross-link between the conserved cysteines, while reduced peptides (red) do not. All values are the mean of ≥3 experiments. Standard deviations were 20% to 25% of the values listed.

[c]MelP5 is a lytic control peptide derived from the bee venom toxin, melittin (23).

[d]Polymer-cushioned, surface-supported PC bilayers on silicon (see the text).

most active in PC vesicles, but its LIC_{50} value is 1:60. $E40_{ox}$, $E17_{ox}$, and $E15_{ox}$ also have detectable activity against PC vesicles but have LIC_{50} values of ≥1:10 (Fig. 5C and Table 2). These results support the conclusion that the delta peptides form ion-permeable pores, but not large pores, in zwitterionic membranes at low concentrations. At higher concentrations, pores are able to release small molecules.

Some viroporins act on internal membranes (18, 19, 28), which have a larger amount of anionic lipids than the plasma membrane, which has mostly zwitterionic lipids. Therefore, we also measured the effects of anionic lipids on delta peptide activity against lipid vesicles. When the vesicles contained 30% or 50% anionic phosphatidylglycerol (PG), the activity of Ebola virus delta peptides increased dramatically, probably due to better binding of the cationic peptides to the anionic bilayers. The LIC_{50} for $E23_{ox}$ decreased 5-fold in the presence of 50% PG compared to PC vesicles, while the LIC_{50} for $E40_{ox}$ and the other delta peptides decreased more than 200-fold (Table 2 and Fig. 5D). Peptide activity increased with increasing PG content. Even reduced peptides showed low activity against 50% PG-containing bilayers, suggesting that strong binding can drive delta peptides into a partially active conformation without the disulfide cross-link. These results suggest that the potency of delta peptides for permeabilizing internal cell membranes could be much higher than the potency we have measured here for plasma membrane permeabilization.

Delta peptides are a conserved part of the EBOV life cycle. In cell culture, sGP and delta peptide are produced by cells transfected with the wild-type EBOV GP RNA (15). The delta peptide associates with cells but is also found in the cell culture supernatant (15), where it is O-glycosylated, likely on threonine 5 and/or threonine 9 (Fig. 2). Radoshitzky and colleagues tested the effects of delta peptide-F_c domain chimeras, added externally, on cell viability and on cell entry by Ebola, Reston, and Marburg viruses or pseudoviruses (29). They noted no direct toxic effect on cells but showed that the chimeras inhibited the entry of all filoviruses, including Marburg. The RESTV delta peptide-F_c chimera did not block filovirus entry, suggesting that the Ebola virus delta peptide has a unique or more potent activity, consistent with the observations we have made here. We have noted elsewhere (30) that many membrane-interacting peptides inhibit the entry of enveloped viruses into cells. Thus, the reported entry inhibition is consistent with the cell-permeabilizing activity that we report here.

Several studies have explored the effect of altering the 7U editing site in the GP gene. In cell culture, recombinant EBOV, in which the editing site and sGP production were eliminated by silent mutation, produced an increased amount of viral GP, and this was linked to higher levels of cytotoxicity and reduced plaque size (31). The RNA-editing site in the Ebola virus GP gene can also undergo rapid evolution, so its continued presence in the viral genome indicates that it has an important functional role that is subject to constant selection pressure. In Vero E6 cells in culture (32, 33), recombinant

EBOV with an additional uridine at the editing site (EBOV/8U, which produces mostly viral GP) appeared after passage and showed a distinct growth advantage over the wild-type EBOV/7U. After 4 or 5 passages in Vero E6 cells, EBOV/8U replaced wild-type EBOV/7U, suggesting that the production of sGP and delta peptide has a fitness cost in cell culture that may exceed the cytotoxicity resulting from increased viral GP production.

On the other hand, in guinea pigs (32) and in nonhuman primates (33, 34), EBOV/8U quickly reverts to wild-type EBOV/7U, while EBOV/7U-infected animals retain the EBOV/7U genotype. Thus, i*n vivo* selection pressure in both rodents and primates strongly favors EBOV/7U, the genotype that produces mostly sGP and delta peptide. A significant amount of sequence data is available from the human outbreak of the Makona variant of Ebola virus in West Africa (21, 35). These data show that the 7 consecutive uridines comprising the RNA-editing site in the GP gene (EBOV/7U) are the dominant genotype in human patients at all stages of infection. The 8U genotype is rarely found. Deep sequencing showed that 99% of mRNAs contained 7A, encoding sGP and delta peptide, while only 1% of mRNAs were 8A, encoding the viral GP.

Ultimately, it is not possible, with current data, to decouple selection pressures on delta peptide production from those on viral GP and on soluble-GP production. Animal studies using viruses with genetically modified GP genes may be needed to address this question. In any case, the genotype that is strongly favored in experimental animal models and in human patients drives the production of delta peptide in large amounts. Further, we have shown here that the active portions of the delta peptide are stable indefinitely against proteolysis in human serum. The redox potential of extracellular fluids strongly supports the formation and maintenance of oxidized disulfide bonds (36). Thus, if delta peptides act extracellularly, they will persist for long periods in the extracellular space and will probably remain locally concentrated in viremic tissues due to cell binding. If delta peptides act intracellularly, they will likely also be stable against cytosolic proteolysis.

Plasma concentrations of delta peptide are unknown; however, plasma concentrations of 34 μg/ml ($\sim$1 μM) sGP in Guinea pigs have been reported, and the amount increases during infection (37). This observation supports the idea that large amounts of sGP and delta peptide are produced. Furthermore, the delta peptide is not likely to be homogeneously distributed. It binds strongly to cells and likely remains concentrated in tissues with an abundance of infected cells, at least for some time. Thus, local concentration (for example, in the intestinal tract epithelia) could easily reach tens of micromoles or higher. Furthermore, delta peptides may act intracellularly, where their local concentration would clearly be high enough to observe the effects we report here.

EBOV delta peptide is a viroporin. Whether they act intracellularly or extracellularly, our results support the hypothesis (16) that Ebola virus delta peptides are viroporins, nonstructural virus-encoded proteins that permeabilize cellular or viral membranes. Well-described viroporins are known from influenza virus, HIV, picornaviruses, rotaviruses, coronaviruses, and others, while putative viroporins have been reported for many other viruses (18, 19, 38–40). Viroporins can act intracellularly to permeabilize organelle membranes (41), modulate calcium homeostasis (42), alter organelle acidification (43), induce autophagy (44), and otherwise "customize host cells for efficient viral propagation" (41). Other viroporins may act extracellularly and permeabilize infected or noninfected cells (18). Here, we show that the delta peptides of Ebola virus are viroporins that indiscriminately permeabilize mammalian cell plasma membranes at micromolar concentrations by altering permeation of ionic compounds and small molecules. This type of behavior has been well described for some viroporins, including the NSP4 enterotoxic viroporin from rotavirus, which increases the ionic permeability of cell membranes without acute lysis (45). Even a small disruption of the ionic permeability of cell membranes is sufficient to disrupt cell function (45) and contribute to viral pathology through intracellular or extracellular effects. Although much remains to be learned, we hypothesize that Ebola virus delta peptides may act on

multiple timescales. First, on the shortest time scale of minutes to hours, the permeabilization of cell membranes will cause disruption of cell function by processes such as dissipation of ion gradients or influx of divalent cations. On longer timescales, even low levels of continuous membrane disruption will lead to cell death.

Finally, we speculate that the viroporin activity of the Ebola virus delta peptide could give it enterotoxic activity. This activity, which would be similar to the activity of the NSP4 enterotoxic viroporin of rotavirus, could be associated with the severe gastrointestinal illness experienced by EVD patients. The resulting vomiting and diarrhea could, in turn, be related to the high efficiency of the Ebola virus Makona variant in spreading to the physical contacts of infected patients (8), including especially family and health care workers. If this speculation is correct, then the viroporin activity of the Ebola virus delta peptide could be a critical, and targetable, part of Ebola virus disease pathology in humans.

MATERIALS AND METHODS

Peptides. All peptides were synthesized by Bio-Synthesis, Inc. Purity and identity were verified with matrix-assisted laser desorption ionization (MALDI) mass spectrometry and reverse-phase high-performance liquid chromatography (HPLC). To oxidize the disulfide bond, peptides were dissolved at <1 mg/ml in 0.025% acetic acid, followed by addition of 20% (vol/vol) dimethyl sulfoxide (DMSO) for 24 h to drive oxidation. Successful oxidation ($>95\%$) and lack of intermolecular cross-links ($<5\%$) were verified with reverse-phase HPLC. Oxidized and reduced peptides, as well as cross-linked multimers, have unique retention times. After oxidation, water and DMSO were removed under high vacuum, and a concentrated peptide stock was made by redissolving in buffer.

Serum stability. $E40_{ox}$ with a C-terminal lysine-biotin residue was incubated at 50 μM with 10% non-heat-treated human serum for 1, 8, and 24 h at 37°C with mixing. The biotinylated peptide was then pulled down with an excess of resin-immobilized streptavidin. After extensive washing of the resin, 1 mM free biotin was added to release biotinylated delta peptide. The collected material was subjected to reverse-phase HPLC and MALDI mass spectrometry. By HPLC and MALDI, mock samples with no delta peptide, but treated identically, contained no detectable peptides. Delta peptide-containing samples showed a cluster of overlapping peaks on HPLC, which corresponded to a cluster of distinct masses on MALDI. Each peak corresponded closely to a potassium adduct of an expected delta peptide fragment. Further, since the fragments were clustered in the 14- to 20-residue range and differed by 1 or 2 residues, peak identification was verified by stepwise sequencing of the peak cluster.

Cell permeation. Cells were seeded into 96-well tissue culture plates and grown to 80 to 90% confluence for 24 to 48 h in full medium. The growth medium was then exchanged for medium lacking fetal bovine serum (FBS) for assays. In a few experiments, 15 min before the addition of peptide, cells were incubated with 1 μM CAMRO for 10 min, followed by washing and replacement of medium. At this point, the cell cytosol was brightly fluorescent. Five minutes before the assay, 100 nM Sytox green was added. Peptides were first serially diluted and then added to the cells at time zero. The Sytox intensity in each well was measured every 5 min for at least 1 h. Sytox green fluorescence at 60 min was used to calculate fractional permeabilization of the plasma membrane.

Cytotoxicity. Vero green monkey cells were grown in 96-well plates as described above. Serially diluted peptide was added, and the cells were incubated at 37°C for 24 h. At that time, 100 nM alamarBlue was added, and any live cells were given 4 h to convert it to the fluorescent product, which was measured in a Biotek Synergy plate reader. The controls for 0% and 100% viability were medium only without cells and cells with no peptide, respectively.

TEER. MDCKII cells were seeded on collagen I-coated polyester transwells after a 1.5-h preincubation with medium to fill the transwell membrane pores, as described previously (46), and cultured for 3 days with the medium changed daily. On the day of the experiment, the cells were washed, incubated in fresh medium for 2 h, and then washed and incubated with 1× CMPBS (1× phosphate-buffered saline [PBS], 0.5 mM $MgCl_2$, 0.75 mM $CaCl_2$) for 40 min. Peptides, diluted in 1× CMPBS in LoBind Eppendorf tubes, were added to the apical compartment, and the cells were incubated at 37°C and 5% CO_2 for 1 h. Following replacement of the peptide solution with CMPBS, the TEER was measured with an EVOM-2 m and Endohm-6 chamber made by World Precision Instruments. TEER is expressed as the difference in resistance between the cell monolayer and blank wells. The effect of peptide is expressed as a fractional loss of TEER 1 h after the addition of peptide.

Hemolysis. Fresh human red blood cells were obtained from Interstate Blood Bank, Inc., and thoroughly washed with PBS until the supernatant was clear. To measure hemolysis, serial dilutions of peptide were prepared and added to 2×10^8 RBC/ml. After incubation for 1 h at 37°C, the cells were centrifuged, and the released hemoglobin was measured by optical absorbance of the heme group (410 nm). The negative control was buffer only (0% lysis), and the positive control was distilled water (100% lysis).

Electrochemical impedance spectroscopy. Impedance measurements were made using a three-electrode system with a silver/silver chloride reference electrode and a platinum counterelectrode. Experimental details were published previously (47). The physisorbed bottom monolayer was made from 1-palmitoyl-2-oleoyl-sn-glycero-3-phosphocholine (POPC) with 5% polyethylene glycol 2000 (PEG-2000) lipids. The upper monolayer was formed by fusion with pure POPC vesicles. The impedance was

measured over the frequency range from 10^5 to 1 Hz using a 20-mV alternating perturbation. The potential was 0 V with respect to the reference electrode. Spectra were recorded at 2-min intervals and fitted to an equivalent circuit model to determine the values of resistance and capacitance of the semiconductor-liquid interface and the bilayer membrane.

Vesicle permeabilization. Large unilamellar vesicles were made by extrusion from POPC and, in some experiments, 1-palmitoyl-2-oleoyl-sn-glycero-3-phosphoglycerol (POPG). Vesicles contained the dye ANTS (6 mM) and its quencher, DPX (12 mM), in 10 mM phosphate buffer as described previously (48). The external solution contained equimolar NaCl at 40 mM in 10 mM phosphate buffer. Peptide serial dilutions were made in LoBind Eppendorf tubes, followed by addition to 0.5 mM lipid vesicles in the wells of a 96-well plate. After 1 h, ANTS fluorescence was measured on a Biotek Synergy plate reader. Fractional leakage was calculated relative to buffer only (0% leakage) and Triton X-100 or MelP5 at a P/L ratio of 1:100 (100% leakage).

ACKNOWLEDGMENTS

This work was supported in part by grants 1R21AI119104 and 1R01GM111824 to W.C.W.; by grants 1U19AI109762, 1R01AI104621, and 2R44AI088843 to R.F.G.; by contracts HHSN272201000022C (principal investigator [PI], Pardis Sabeti), HHSN272200900049C (PI: James Robinson), and HHSN27220140048C (PI, Michael Oldstone), for which R.F.G. is an investigator; by grant NSF MCB 1157687 to K.H.; and by grant DTRA (HDTRA1-15-1-0046) to P.C.S. T.F. is supported by NIH F31 CA188662. A.K. is supported by NIH T32 CA153952.

W.C.W., K.H., R.F.G., and W.R.G. designed experiments, analyzed data, and wrote the manuscript. J.H. and L.I.M. designed and performed experiments, analyzed data, and edited the manuscript. P.C.S. designed impedance and TEER experiments and edited the manuscript. All the other authors performed experiments, analyzed data, and edited the manuscript.

REFERENCES

1. Mari Saéz A, Weiss S, Nowak K, Lapeyre V, Zimmermann F, Dux A, Kuhl HS, Kaba M, Regnaut S, Merkel K, Sachse A, Thiesen U, Villanyi L, Boesch C, Dabrowski PW, Radonic A, Nitsche A, Leendertz SA, Petterson S, Becker S, Krahling V, Couacy-Hymann E, Akoua-Koffi C, Weber N, Schaade L, Fahr J, Borchert M, Gogarten JF, Calvignac-Spencer S, Leendertz FH. 2015. Investigating the zoonotic origin of the West African Ebola epidemic. EMBO Mol Med 7:17–23. https://doi.org/10.15252/emmm.201404792.
2. World Health Organization. 2016. Ebola situation report. World Health Organization, Geneva, Switzerland.
3. Uyeki TM, Erickson BR, Brown S, McElroy AK, Cannon D, Gibbons A, Sealy T, Kainulainen MH, Schuh AJ, Kraft CS, Mehta AK, Lyon GM, Varkey JB III, Ribner BS, Ellison RT, Carmody E III, Nau GJ, Spiropoulou C, Nichol ST, Stroher U. 2016. Ebola virus persistence in semen of male survivors. Clin Infect Dis 62:1552–1555. https://doi.org/10.1093/cid/ciw202.
4. Varkey JB, Shantha JG, Crozier I, Kraft CS, Lyon GM, Mehta AK, Kumar G, Smith JR, Kainulainen MH, Whitmer S, Stroher U, Uyeki TM, Ribner BS, Yeh S. 2015. Persistence of Ebola virus in ocular fluid during convalescence. N Engl J Med 372:2423–2427. https://doi.org/10.1056/NEJMoa1500306.
5. Sissoko D, Keita M, Diallo B, Aliabadi N, Fitter DL, Dahl BA, Bore JA, Koundouno FR, Singethan K, Meisel S, Enkirch T, Mazzarelli A, Amburgey V, Faye O, Sall AA, Magassouba N, Carroll MW, Anglaret X, Malvy D, Formenty P, Aylward RB, Keita S, Djingarey MH, Loman NJ, Gunther S, Duraffour S. 2017. Ebola virus persistence in breast milk after no reported illness: a likely source of virus transmission from mother to child. Clin Infect Dis 64:513–516. https://doi.org/10.1093/cid/ciw793.
6. Jacobs M, Rodger A, Bell DJ, Bhagani S, Cropley I, Filipe A, Gifford RJ, Hopkins S, Hughes J, Jabeen F, Johannessen I, Karageorgopoulos D, Lackenby A, Lester R, Liu RS, MacConnachie A, Mahungu T, Martin D, Marshall N, Mepham S, Orton R, Palmarini M, Patel M, Perry C, Peters SE, Porter D, Ritchie D, Ritchie ND, Seaton RA, Sreenu VB, Templeton K, Warren S, Wilkie GS, Zambon M, Gopal R, Thomson EC. 2016. Late Ebola virus relapse causing meningoencephalitis: a case report. Lancet 388:498–503. https://doi.org/10.1016/S0140-6736(16)30386-5.
7. Diallo B, Sissoko D, Loman NJ, Bah HA, Bah H, Worrell MC, Conde LS, Sacko R, Mesfin S, Loua A, Kalonda JK, Erondu NA, Dahl BA, Handrick S, Goodfellow I, Meredith LW, Cotten M, Jah U, Guetiya Wadoum RE, Rollin P, Magassouba N, Malvy D, Anglaret X, Carroll MW, Aylward RB, Djingarey MH, Diarra A, Formenty P, Keita S, Gunther S, Rambaut A, Duraffour S. 2016. Resurgence of Ebola virus disease in Guinea linked to a survivor with virus persistence in seminal fluid for more than 500 days. Clin Infect Dis 63:1353–1356. https://doi.org/10.1093/cid/ciw601.
8. Schieffelin JS, Shaffer JG, Goba A, Gbakie M, Gire SK, Colubri A, Sealfon RS, Kanneh L, Moigboi A, Momoh M, Fullah M, Moses LM, Brown BL, Andersen KG, Winnicki S, Schaffner SF, Park DJ, Yozwiak NL, Jiang PP, Kargbo D, Jalloh S, Fonnie M, Sinnah V, French I, Kovoma A, Kamara FK, Tucker V, Konuwa E, Sellu J, Mustapha I, Foday M, Yillah M, Kanneh F, Saffa S, Massally JL, Boisen ML, Branco LM, Vandi MA, Grant DS, Happi C, Gevao SM, Fletcher TE, Fowler RA, Bausch DG, Sabeti PC, Khan SH, Garry RF. 2014. Clinical illness and outcomes in patients with Ebola in Sierra Leone. N Engl J Med 371:2092–2100. https://doi.org/10.1056/NEJMoa1411680.
9. Bah EI, Lamah MC, Fletcher T, Jacob ST, Brett-Major DM, Sall AA, Shindo N, Fischer WA, Lamontagne F, Saliou SM, Bausch DG, Moumie B, Jagatic T, Sprecher A, Lawler JV, Mayet T, Jacquerioz FA, Mendez Baggi MF, Vallenas C, Clement C, Mardel S, Faye O, Faye O, Soropogui B, Magassouba N, Koivogui L, Pinto R, Fowler RA. 2015. Clinical presentation of patients with Ebola virus disease in Conakry, Guinea. N Engl J Med 372:40–47. https://doi.org/10.1056/NEJMoa1411249.
10. Henao-Restrepo AM, Camacho A, Longini IM, Watson CH, Edmunds WJ, Egger M, Carroll MW, Dean NE, Diatta I, Doumbia M, Draguez B, Duraffour S, Enwere G, Grais R, Gunther S, Gsell PS, Hossmann S, Watle SV, Konde MK, Keita S, Kone S, Kuisma E, Levine MM, Mandal S, Mauget T, Norheim G, Riveros X, Soumah A, Trelle S, Vicari AS, Rottingen JA, Kieny MP. 2017. Efficacy and effectiveness of an rVSV-vectored vaccine in preventing Ebola virus disease: final results from the Guinea ring vaccination, open-label, cluster-randomised trial. Lancet 389:505–518. https://doi.org/10.1016/S0140-6736(16)32621-6.
11. Sanchez A, Trappier SG, Mahy BW, Peters CJ, Nichol ST. 1996. The virion glycoproteins of Ebola viruses are encoded in two reading frames and are expressed through transcriptional editing. Proc Natl Acad Sci U S A 93:3602–3607. https://doi.org/10.1073/pnas.93.8.3602.
12. Volchkova VA, Dolnik O, Martinez MJ, Reynard O, Volchkov VE. 2015. RNA editing of the GP gene of Ebola virus is an important pathogenicity factor. J Infect Dis 212(Suppl 2):S226–S233. https://doi.org/10.1093/infdis/jiv309.
13. Volchkova VA, Feldmann H, Klenk HD, Volchkov VE. 1998. The nonstructural small glycoprotein sGP of Ebola virus is secreted as an antiparallel-orientated homodimer. Virology 250:408–414. https://doi.org/10.1006/viro.1998.9389.

14. Mohan GS, Li W, Ye L, Compans RW, Yang C. 2012. Antigenic subversion: a novel mechanism of host immune evasion by Ebola virus. PLoS Pathog 8:e1003065. https://doi.org/10.1371/journal.ppat.1003065.
15. Volchkova VA, Klenk HD, Volchkov VE. 1999. Delta-peptide is the carboxy-terminal cleavage fragment of the nonstructural small glycoprotein sGP of Ebola virus. Virology 265:164–171. https://doi.org/10.1006/viro.1999.0034.
16. Gallaher WR, Garry RF. 2015. Modeling of the Ebola virus delta peptide reveals a potential lytic sequence motif. Viruses 7:285–305. https://doi.org/10.3390/v7010285.
17. Wimley WC. 2010. Describing the mechanism of antimicrobial peptide action with the interfacial activity model. ACS Chem Biol 5:905–917. https://doi.org/10.1021/cb1001558.
18. Nieva JL, Madan V, Carrasco L. 2012. Viroporins: structure and biological functions. Nat Rev Microbiol 10:563–574. https://doi.org/10.1038/nrmicro2820.
19. Nieto-Torres JL, Verdia-Baguena C, Castano-Rodriguez C, Aguilella VM, Enjuanes L. 2015. Relevance of viroporin ion channel activity on viral replication and pathogenesis. Viruses 7:3552–3573. https://doi.org/10.3390/v7072786.
20. Yount NY, Yeaman MR. 2004. Multidimensional signatures in antimicrobial peptides. Proc Natl Acad Sci U S A 101:7363–7368. https://doi.org/10.1073/pnas.0401567101.
21. Gire SK, Goba A, Andersen KG, Sealfon RS, Park DJ, Kanneh L, Jalloh S, Momoh M, Fullah M, Dudas G, Wohl S, Moses LM, Yozwiak NL, Winnicki S, Matranga CB, Malboeuf CM, Qu J, Gladden AD, Schaffner SF, Yang X, Jiang PP, Nekoui M, Colubri A, Coomber MR, Fonnie M, Moigboi A, Gbakie M, Kamara FK, Tucker V, Konuwa E, Saffa S, Sellu J, Jalloh AA, Kovoma A, Koninga J, Mustapha I, Kargbo K, Foday M, Yillah M, Kanneh F, Robert W, Massally JL, Chapman SB, Bochicchio J, Murphy C, Nusbaum C, Young S, Birren BW, Grant DS, Scheiffelin JS, Lander ES, Happi C, Gevao SM, Gnirke A, Rambaut A, Garry RF, Khan SH, Sabeti PC. 2014. Genomic surveillance elucidates Ebola virus origin and transmission during the 2014 outbreak. Science 345:1369–1372. https://doi.org/10.1126/science.1259657.
22. Miranda ME, Miranda NL. 2011. Reston ebolavirus in humans and animals in the Philippines: a review. J Infect Dis 204(Suppl 3):S757–S760. https://doi.org/10.1093/infdis/jir296.
23. Krauson AJ, He J, Wimley WC. 2012. Gain-of-function analogues of the pore-forming peptide melittin selected by orthogonal high-throughput screening. J Am Chem Soc 134:12732–12741. https://doi.org/10.1021/ja3042004.
24. Aleksandrowicz P, Marzi A, Biedenkopf N, Beimforde N, Becker S, Hoenen T, Feldmann H, Schnittler HJ. 2011. Ebola virus enters host cells by macropinocytosis and clathrin-mediated endocytosis. J Infect Dis 204(Suppl 3):S957–S967. https://doi.org/10.1093/infdis/jir326.
25. Wiedman G, Fuselier T, He J, Searson PC, Hristova K, Wimley WC. 2014. Highly efficient macromolecule-sized poration of lipid bilayers by a synthetically evolved peptide. J Am Chem Soc 136:4724–4731. https://doi.org/10.1021/ja500462s.
26. DeGrado WF, Musso GF, Lieber M, Kaiser ET, Kézdy FJ. 1982. Kinetics and mechanism of hemolysis induced by melittin and by a synthetic melittin analogue. Biophys J 37:329–338. https://doi.org/10.1016/S0006-3495(82)84681-X.
27. Lin J, Merzlyakov M, Hristova K, Searson PC. 2008. Impedance spectroscopy of bilayer membranes on single crystal silicon. Biointerphases 3:FA33. https://doi.org/10.1116/1.2896117.
28. Nieva JL, Agirre A, Nir S, Carrasco L. 2003. Mechanisms of membrane permeabilization by picornavirus 2B viroporin. FEBS Lett 552:68–73. https://doi.org/10.1016/S0014-5793(03)00852-4.
29. Radoshitzky SR, Warfield KL, Chi X, Dong L, Kota K, Bradfute SB, Gearhart JD, Retterer C, Kranzusch PJ, Misasi JN, Hogenbirk MA, Wahl-Jensen V, Volchkov VE, Cunningham JM, Jahrling PB, Aman MJ, Bavari S, Farzan M, Kuhn JH. 2011. Ebolavirus delta-peptide immunoadhesins inhibit marburgvirus and ebolavirus cell entry. J Virol 85:8502–8513. https://doi.org/10.1128/JVI.02600-10.
30. Badani H, Garry RF, Wimley WC. 2014. Peptide entry inhibitors of enveloped viruses: the importance of interfacial hydrophobicity. Biochim Biophys Acta 1838:2180–2197. https://doi.org/10.1016/j.bbamem.2014.04.015.
31. Volchkov VE, Volchkova VA, Muhlberger E, Kolesnikova LV, Weik M, Dolnik O, Klenk HD. 2001. Recovery of infectious Ebola virus from complementary DNA: RNA editing of the GP gene and viral cytotoxicity. Science 291:1965–1969. https://doi.org/10.1126/science.1057269.
32. Volchkova VA, Dolnik O, Martinez MJ, Reynard O, Volchkov VE. 2011. Genomic RNA editing and its impact on Ebola virus adaptation during serial passages in cell culture and infection of guinea pigs. J Infect Dis 204(Suppl 3):S941–S946. https://doi.org/10.1093/infdis/jir321.
33. Kugelman JR, Lee MS, Rossi CA, McCarthy SE, Radoshitzky SR, Dye JM, Hensley LE, Honko A, Kuhn JH, Jahrling PB, Warren TK, Whitehouse CA, Bavari S, Palacios G. 2012. Ebola virus genome plasticity as a marker of its passaging history: a comparison of in vitro passaging to non-human primate infection. PLoS One 7:e50316. https://doi.org/10.1371/journal.pone.0050316.
34. Trefry JC, Wollen SE, Nasar F, Shamblin JD, Kern SJ, Bearss JJ, Jefferson MA, Chance TB, Kugelman JR, Ladner JT, Honko AN, Kobs DJ, Wending MQ, Sabourin CL, Pratt WD, Palacios GF, Pitt ML. 2015. Ebola virus infections in nonhuman primates are temporally influenced by glycoprotein poly-U editing site populations in the exposure material. Viruses 7:6739–6754. https://doi.org/10.3390/v7122969.
35. Folarin OA, Ehichioya D, Schaffner SF, Winnicki SM, Wohl S, Eromon P, West KL, Gladden-Young A, Oyejide NE, Matranga CB, Deme AB, James A, Tomkins-Tinch C, Onyewurunwa K, Ladner JT, Palacios G, Nosamiefan I, Andersen KG, Omilabu S, Park DJ, Yozwiak NL, Nasidi A, Garry RF, Tomori O, Sabeti PC, Happi CT. 2016. Ebola virus epidemiology and evolution in Nigeria. J Infect Dis 214:S102–S109. https://doi.org/10.1093/infdis/jiw190.
36. Ottaviano FG, Handy DE, Loscalzo J. 2008. Redox regulation in the extracellular environment. Circ J 72:1–16. https://doi.org/10.1253/circj.72.1.
37. Escudero-Perez B, Volchkova VA, Dolnik O, Lawrence P, Volchkov VE. 2014. Shed GP of Ebola virus triggers immune activation and increased vascular permeability. PLoS Pathog 10:e1004509. https://doi.org/10.1371/journal.ppat.1004509.
38. Largo E, Gladue DP, Huarte N, Borca MV, Nieva JL. 2014. Pore-forming activity of pestivirus p7 in a minimal model system supports genus-specific viroporin function. Antiviral Res 101:30–36. https://doi.org/10.1016/j.antiviral.2013.10.015.
39. Giorda KM, Raghava S, Zhang MW, Hebert DN. 2013. The viroporin activity of the minor structural proteins VP2 and VP3 is required for SV40 propagation. J Biol Chem 288:2510–2520. https://doi.org/10.1074/jbc.M112.428425.
40. Sanchez-Martinez S, Madan V, Carrasco L, Nieva JL. 2012. Membrane-active peptides derived from picornavirus 2B viroporin. Curr Protein Pept Sci 13:632–643. https://doi.org/10.2174/138920312804142165.
41. Giorda KM, Hebert DN. 2013. Viroporins customize host cells for efficient viral propagation. DNA Cell Biol 32:557–564. https://doi.org/10.1089/dna.2013.2159.
42. Hyser JM, Utama B, Crawford SE, Broughman JR, Estes MK. 2013. Activation of the endoplasmic reticulum calcium sensor STIM1 and store-operated calcium entry by rotavirus requires NSP4 viroporin activity. J Virol 87:13579–13588. https://doi.org/10.1128/JVI.02629-13.
43. Grigoryan G, Moore DT, DeGrado WF. 2011. Transmembrane communication: general principles and lessons from the structure and function of the M2 proton channel, K(+) channels, and integrin receptors. Annu Rev Biochem 80:211–237. https://doi.org/10.1146/annurev-biochem-091008-152423.
44. Crawford SE, Estes MK. 2013. Viroporin-mediated calcium-activated autophagy. Autophagy 9:797–798. https://doi.org/10.4161/auto.23959.
45. Hyser JM, Collinson-Pautz MR, Utama B, Estes MK. 2010. Rotavirus disrupts calcium homeostasis by NSP4 viroporin activity. mBio 1:e00265-10. https://doi.org/10.1128/mBio.00265-10.
46. Gallagher E, Minn I, Chambers JE, Searson PC. 2016. In vitro characterization of pralidoxime transport and acetylcholinesterase reactivation across MDCK cells and stem cell-derived human brain microvascular endothelial cells (BC1-hBMECs). Fluids Barriers CNS 13:10. https://doi.org/10.1186/s12987-016-0035-0.
47. Lin J, Szymanski J, Searson PC, Hristova K. 2010. Effect of a polymer cushion on the electrical properties and stability of surface-supported lipid bilayers. Langmuir 26:3544–3548. https://doi.org/10.1021/la903232b.
48. Wimley WC. 2015. Determining the effects of membrane-interacting peptides on membrane integrity. Methods Mol Biol 1324:89–106. https://doi.org/10.1007/978-1-4939-2806-4_6.